Linear-to-Circular Polarizers for Multi-Octave Bandwidths and Wide Scan Angles at mm-Wave Frequencies Using Rotated Anisotropic Layers

Carl Pfeiffer[1, 2, *] and Boris Tomasic[2]

Abstract—Linear-to-circular polarizers operating from roughly 17 to 65 GHz, and angles of incidence up to 60° are reported. These polarizers convert incident linearly polarized radiation into circular polarization upon transmission. First, previous designs inspired by the optics community using cascaded waveplates are scaled down to mm-wave frequencies. The naturally occurring anisotropic crystals that the optics community employed are replaced here with metamaterials. The range of incidence angles is improved by utilizing biaxial artificial dielectrics whose permittivity in the x, y and z directions are all engineered. Next, an ultra-wideband linear-to-circular polarizer consisting of cascaded sheet impedances is reported. The cascaded sheet impedance polarizer utilizes a combination of meanderline and metallic patch geometries. The principal axes of each patterned metallic sheet are oriented at an optimized angle, which increases the design degrees of freedom and performance. This polarizer has the advantages of being thinner and easier to fabricate than the polarizer utilizing cascaded waveplates, but is more difficult to design. Both polarizers rely heavily on genetic algorithm optimization in the design process to realize multiple octaves of bandwidths and robust performance at wide angles of incidence. The polarizers are fabricated with commercial printed-circuit-boards and then experimentally characterized.

1. INTRODUCTION

Linear-to-circular polarizers convert an incident, linearly polarized plane wave into a transmitted, circularly polarized wave. Linear-to-circular polarizers are commonly utilized from microwave to optical frequencies for a myriad of applications. Many of these applications also demand wide operating bandwidths and wide angles of incidence. However, conventional linear-to-circular polarizers only work perfectly at a single frequency, which make them inherently narrowband. This fact has inspired significant research efforts to extend their bandwidth.

At THz frequencies and higher, wideband linear-to-circular polarizers are typically realized by cascading multiple birefringent waveplates with rotated principal axes [1–3]. Polarizers utilizing cascaded waveplates can realize multiple octaves of bandwidth. At these higher frequencies, the geometry can afford to be many wavelengths in thickness while still maintaining a low profile since the wavelength is short. A disadvantage of these designs is they do not typically work well at wide angles of incidence since the optical thickness of the plate is a function of the angle of incidence.

At microwave frequencies, the most common linear-to-circular polarizers utilize cascaded patterned metallic sheets (i.e., sheet impedances) with subwavelength overall thicknesses [4, 5]. The bandwidth of microwave linear-to-circular polarizers are typically less than 40% [6, 7]. In some examples, the bandwidth has been increased up to an octave using meanderline metallic patterns printed on dielectric

* Corresponding author: Carl Pfeiffer (carlpfei@umich.edu).

[1] Defense Engineering Corporation, 4027 Colonel Glenn Hwy, Beavercreek, OH 45431, USA. [2] Air Force Research Laboratory, Sensors Directorate, 2241 Avionics Circle, Wright-Patterson AFB, OH 45433-7320, USA.

substrates [8, 9]. However, these meanderline polarizers do not typically work well at wide angles of incidence when their bandwidth is large [10]. Other recently proposed structures also provide a similar performance as meanderline metallic polarizers [11]. Alternatively, polarizers operating in reflection mode have recently been designed with two octaves of bandwidth [12], and multi-band operation [13].

Here, we aim to develop linear-to-circular polarizers at mm-wave frequencies that realize multiple octaves of bandwidth, while also working at wide angles of incidence. Approaches inspired by both optics and microwave engineering communities are considered. First, an approach inspired by the optics community is used, where the polarizer consists of cascaded waveplates. Rather than utilizing naturally materials, each waveplate is realized with artificial anisotropic dielectrics. The polarizer is designed to work at significantly wider angles of incidence than the state-of-the-art by engineering the permittivity in the x, y, and z directions. Next, a polarizer inspired by the microwave engineering community is proposed, which consists of cascaded sheet impedances. In contrast to previous designs, the polarizer utilizes metallic patterns shaped as both meanderline and patch geometries. Furthermore, the principal axes of each sheet are rotated by optimized angles to increase the degrees of freedom and performance. This cascaded sheet impedance polarizer is easier to fabricate and thinner than the cascaded waveplate polarizer. Both polarizers are designed using a genetic algorithm optimization process, and their simulated and measured performances are reported. Finally, it is shown that it is possible to refine the performance of a fabricated prototype by 3D printing a dielectric grating that compensates for fabrication tolerances.

2. BACKGROUND AND DEFINITIONS

To begin, it is useful to define some metrics used to characterize the performance of linear-to-circular polarizers. Consider an arbitrary structure illuminated with a normally incident plane wave. The linearly polarized transmission matrix ($\mathbf{T}^{LIN}$) of the structure relates the incident electric field E_i to the transmitted electric field E_t,

$$\begin{pmatrix} E_t^x \\ E_t^y \end{pmatrix} = \mathbf{T}^{LIN} \begin{pmatrix} E_i^x \\ E_i^y \end{pmatrix} = e^{-j\delta} \begin{pmatrix} T_{xx} & T_{xy} \\ T_{yx} & T_{yy} \end{pmatrix} \begin{pmatrix} E_i^x \\ E_i^y \end{pmatrix} \tag{1}$$

where δ is an constant phase shift [14]. Without loss of generality, an ideal linear-to-circular polarizer converts an incident x-polarization to a transmitted right-handed circular polarization. In other words, $T_{xx} = 1/\sqrt{2}$ and $T_{yx} = -\mathrm{j}/\sqrt{2}$. It is often more convenient to characterize the performance of a linear-to-circular polarizer by considering the linear-to-circular transmission matrix ($\mathbf{T}^{CP}$) which is defined here as,

$$\begin{pmatrix} E_t^R \\ E_t^L \end{pmatrix} = \mathbf{T}^{CP} \begin{pmatrix} E_i^x \\ E_i^y \end{pmatrix} = \begin{pmatrix} T_{Rx} & T_{Ry} \\ T_{Lx} & T_{Ly} \end{pmatrix} \begin{pmatrix} E_i^x \\ E_i^y \end{pmatrix} \tag{2}$$

where R and L denote transmission into right and left handed circular polarizations, respectively. The matrix $\mathbf{T}^{CP}$ is related to $\mathbf{T}^{LIN}$ by,

$$\mathbf{T}^{CP} = \sqrt{2} \begin{pmatrix} 1 & 1 \\ -j & j \end{pmatrix}^{-1} \mathbf{T}^{LIN} \tag{3}$$

Ideally, $T_{Rx} = 1$ and $T_{Lx} = 0$. The polarization purity of the transmitted wave is often expressed in terms of the axial ratio (AR), which can be related to the linear-to-circular transmission matrix by [15],

$$AR = \frac{|T_{Rx}/T_{Lx}| + 1}{|T_{Rx}/T_{Lx}| - 1} \tag{4}$$

Note that a y-polarized incident wave is not considered here. The polarizers proposed here are characterized at different angles of incidence. The E and H planes are defined relative to the plane of the incident wave. In other words the E-plane corresponds to the $\phi = 0°$ plane and the H-plane is the $\phi = 90°$ plane. It should also be noted that the term T_{Rx} is used to characterize transmission of obliquely incident waves as well as normally incident waves. Rigorously speaking, the incident polarization is x-polarized with respect to the third-definition provided by Ludwig [16].

3. DESIGN AND SIMULATION

3.1. Cascaded Waveplate Polarizer

Conventional waveplates composed of uniaxial dielectrics (i.e., $\varepsilon_{xx} = \varepsilon_{zz} \neq \varepsilon_{yy}$) only operate at a single frequency. It has been known since the 1950's that the bandwidth can be significantly extended by cascading waveplates with different thicknesses and relative orientations to develop so-called achromatic waveplates [1]. These waveplates are commercially available at optical frequencies with bandwidths of over 4 : 1 [17]. This design approach has been scaled from optical to submillimeter [2] and mm-wave [3] frequencies. However, as the wavelength is increased further, the required thickness of naturally occurring crystals becomes prohibitive due to the notable weight, size, and loss. Consequently, artificial anisotropic dielectrics (i.e., metamaterials), are considered here.

To begin, let us analyze the simplest linear-to-circular polarizer, which is a single waveplate. Ignoring reflection losses and absorption for the moment, the transmission matrix of a waveplate can be written as,

$$\mathbf{T}_{wp}(\beta d \Delta n) = \mathbf{R}\left(\beta\right)^{-1} \begin{pmatrix} 1 & 0 \\ 0 & e^{-jk_0 d \Delta n} \end{pmatrix} \mathbf{R}(\beta) \tag{5}$$

where $k_0 = \omega\sqrt{\varepsilon_0 \mu_0}$ is the wave impedance of free space, d the thickness of the waveplate, Δn the difference in refrefractive index along the two principal axes and,

$$\mathbf{R} = \begin{pmatrix} \cos(\beta) & -\sin(\beta) \\ \sin(\beta) & \cos(\beta) \end{pmatrix}, \tag{6}$$

is the β-degree rotation matrix. It should be noted that the transmission matrix can be diagonalized using the eigenvectors $\mathbf{u} = \cos(\beta)\mathbf{x} - \sin(\beta)\mathbf{y}$ and $\mathbf{v} = \sin(\beta)\mathbf{x} + \cos(\beta)\mathbf{y}$, where $\mathbf{x}$ and $\mathbf{y}$ are unit vectors. The waveplate orientation, β, and the electrical thickness, $d\Delta n$, are two degrees of freedom that can be adjusted to control T_{Rx} and T_{Lx} at a single frequency to realize a monochromatic linear-to-circular polarizer. The bandwidth can be extended by cascading two waveplates together such that $\mathbf{T}_{cas} = \mathbf{T}_{wp2}(\beta_2 d_2 \Delta n_2)\mathbf{T}_{wp1}(\beta_1 d_1 \Delta n_1)$. Increasing the number of waveplates increases the degrees of freedom, which allows for designing multi-resonant linear-to-circular polarizers that operate perfectly at multiple frequencies. For example, consider the case where two anisotropic dielectrics are cascaded, as shown in Figure 1. The thickness of each layer is 40 mm, which corresponds to $9.3\lambda_h$, where λ_h is the wavelength at the highest operating frequency of 70 GHz. The permittivities of the waveplates are,

$$\varepsilon_1 = \begin{pmatrix} 1.02 & 0.05 & 0 \\ 0.05 & 1.16 & 0 \\ 0 & 0 & 1 \end{pmatrix} \quad \varepsilon_2 = \begin{pmatrix} 1.08 & 0.02 & 0 \\ 0.02 & 1.01 & 0 \\ 0 & 0 & 1 \end{pmatrix} \tag{7}$$

Diagonalizing the permittivities reveals that β_1, $d_1\Delta n_1$, β_2, $d_2\Delta n_2$ equal 17.6°, 3.33 mm, 72.4°, 1.667 mm, respectively. As shown in Figure 1(b), the polarizer works perfectly at the design frequencies of 30 GHz and 60 GHz ($|T_{Rx}| = AR = 0$ dB) and maintains a decent performance between them. The double resonance significantly increases the bandwidth over the case of a single waveplate. Naturally, adding additional waveplates provides more degrees of freedom which can be utilized to enhance bandwidth and/or improve axial ratio throughout the band.

An issue with these cascaded waveplate polarizers is that the performance is typically sensitive to the angle of incidence. Increasing the angle of incidence increases the amount of time a wave spends within the slab, which in turn increases the effective electrical thickness of each layer. For example Figure 1(c) plots the response of the same cascaded waveplates when illuminated at 45° from broadside in the E-plane. The performance is significantly degraded compared to normal incidence since the axial ratio is above 5 dB throughout the band

Two mechanisms are used here to address the sensitivity to oblique angles of incidence. First, the permittivity of the anisotropic material is increased. This bends the wave towards the normal direction as it propagates through the slab in accordance with Snell's law [18]. Therefore, the optical thickness that the wave sees is less dependent upon the angle of incidence For example, if the angle of incidence is 60° and the average permittivity within the waveplates is 3.5, the wave only propagates at 28° within the waveplates. However, impedance matching layers need to be added to the front and back of the material which increases complexity and thickness.
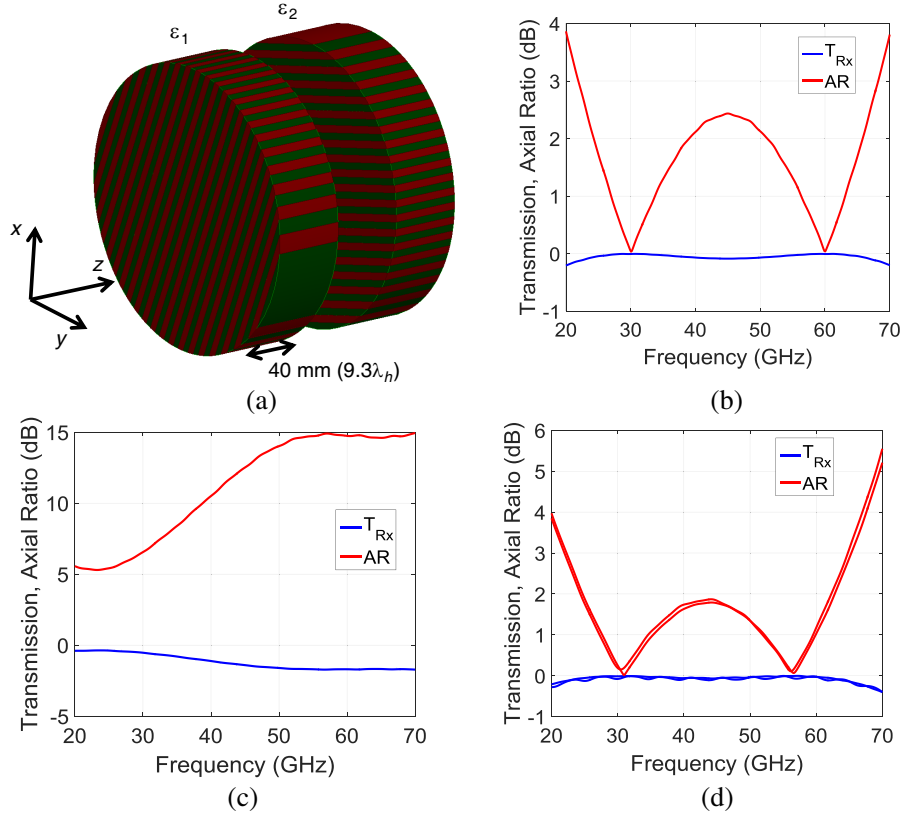
Figure 1. Cascading two waveplates significantly enhances the bandwidth. (a) Two cascaded waveplates designed to convert incident x-polarization to right-handed-circular polarization. The waveplates are oriented at optimized angles. A gap between the waveplates is added to the figure for clarity. (b) and (c) Simulated response of the cascaded waveplates when the permittivity is given by (7), and the waveplates are illuminated at normal incidence and at $45°$ in the E-plane, respectively. The performance is significantly degraded at oblique angles. (d) Simulated response when the permittivities of the two waveplates are given by (8), and the polarizer is illuminated at an angle of incidence of $45°$ in the E- and H-planes. The E-plane and H-plane curves are nearly on top of each other.

Next, the range of incidence angles is increased further by controlling the permittivity in the x, y and z directions. Controlling the permittivity in three principal directions can reduce the index contrast between the two eigenpolarizations at oblique angles, which compensates for the increased optical thickness. For example, if the permittivity in the z-direction is increased such that,

$$\varepsilon_1 = \begin{pmatrix} 1.02 & 0.05 & 0 \\ 0.05 & 1.16 & 0 \\ 0 & 0 & 1.08 \end{pmatrix}, \quad \varepsilon_2 = \begin{pmatrix} 1.08 & 0.02 & 0 \\ 0.02 & 1.01 & 0 \\ 0 & 0 & 1.04 \end{pmatrix} \tag{8}$$

the transmission coefficient and axial ratio at $45°$ scan in the E- and H-planes are shown in Figure 1(d). The response at oblique angles is very similar to the broadside case when the z-directed permittivity is properly chosen. It was generally observed that the z-directed permittivity should be near the geometric mean of the u and v directed permittivities (i.e., the transverse permittivities along the principal axes) if the polarizer is expected to work at wide scan angles.

A section of the designed cascaded waveplate polarizer is shown in Figure 2. The internal section consists of 4 anisotropic artificial dielectric slabs with rotated principal axes. The outer section utilizes 3 dielectric matching layers on either side to impedance match the artificial dielectrics to free space. The thickness and orientation of the different layers are optimized using a genetic algorithm implemented in MATLAB For simplicity, the anisotropic dielectric slabs all have the same permittivity. In total, there
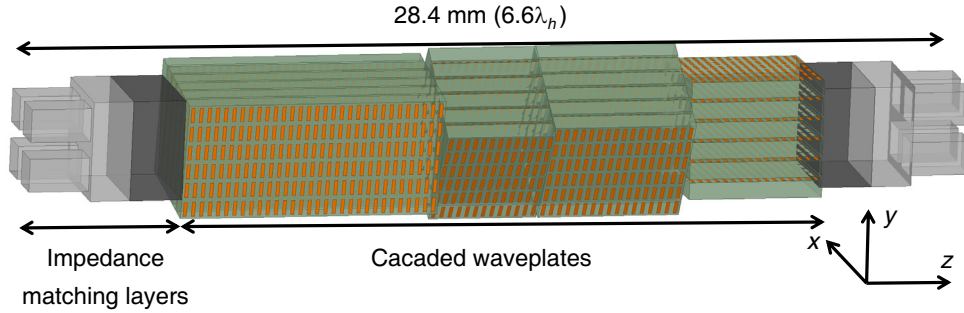
Figure 2. Section of the designed linear-to-circular polarizer realized using cascaded waveplates. The internal region consists of 4 cascaded anisotropic artificial dielectrics. There are 3 dielectric impedance matching layers on either side of the anisotropic waveplates.

are 14 degrees of freedom that need to be optimized: thickness and permittivity of the 3 matching layers (6 unknowns), and thickness and orientation of the 4 anisotropic dielectrics (8 unknowns).

The genetic algorithm optimization begins with an initial population of 200 randomly seeded individuals. The transmission coefficients, $T_{Rx}(\omega, \theta, \phi)$ and $T_{Lx}(\omega, \theta, \phi)$ of each individual are analytically calculated for normal and oblique angles of incidence using expressions provided in the supplementary material of [19]. The individuals with lowest cost are selected from the population, randomly mutated, and the process is repeated. The cost function that is minimized is given by

$$Cost = \sum_{\omega} \left[\left(1 + |T_{Lx}(\omega, 0°, 0°)| - |T_{Rx}(\omega, 0°, 0°)|\right)^5 \right.$$

$$\left. + \sum_{\phi} \left(\frac{\left(1 + |T_{Lx}(\omega, 60°, \phi)| - |T_{Rx}(\omega, 60°, \phi)|\right)^5}{10} \right) \right] \tag{9}$$

This cost function maximizes T_{Rx} and minimizes T_{Lx}, which minimizes insertion loss and axial ratio over the desired bandwidth and angles of incidence. The transmission coefficients are calculated at 21 frequency points between 15 GHz and 70 GHz, and at angles of incidence $\theta = 0°$, $60°$, and $\phi = -45°$, $0°$, $45°$, $60°$. A larger weight is assigned to the transmission coefficients at normal incidence. The summed elements within the cost function $(1 + |T_{Lx}| - |T_{Rx}|)$ are raised to the 5th power, which helps optimize for the worst-case scenario. Of course there are a myriad of other cost functions that could be utilized, which would allow tradeoffs to be made between size, bandwidth, maximum axial ratio, minimum insertion loss and maximum scan angle. The optimization process takes on the order of 30 minutes to complete with a 24 core CPU running at 2.5 GHz.

Once the optimal material permittivities and thicknesses are determined, each layer is physically implemented. The impedance matching layers are physically realized by stacking together different substrates. The effective permittivities of the impedance matching layers shown in Figure 2 are 1.3, 1.8, and 2.2, with thicknesses equal to 1.8 mm, 1.2 mm, and 1.6 mm, respectively. A broadband impedance match between free space and the cascaded waveplates is realized by gradually transitioning the permittivity. The permittivity of the outermost dielectric is reduced from 1.8 to 1.3, by milling trenches in the substrate, as shown in Figure 2.

A unit cell of the cascaded, anisotropic waveplates is shown in Figure 3. It is designed using standard dielectric mixing formulas to realize the optimized anisotropic permittivity [20, 21]. The principal axes of the unit cell are oriented along the u, v, and z directions. Each cell consists of a 0.5 mm thickness Rogers 4003 substrate ($\varepsilon = 3.55$) patterned with a copper patch that is 0.1 mm × 0.45 mm in size. The copper rectangle primarily increases the permittivity in the v direction, while minimally affecting the permittivity in the u and z directions. The small unit cell size reduces the effects of both temporal and spatial dispersion. The effective permittivity tensor of the unit cell was extracted by illuminating a 10
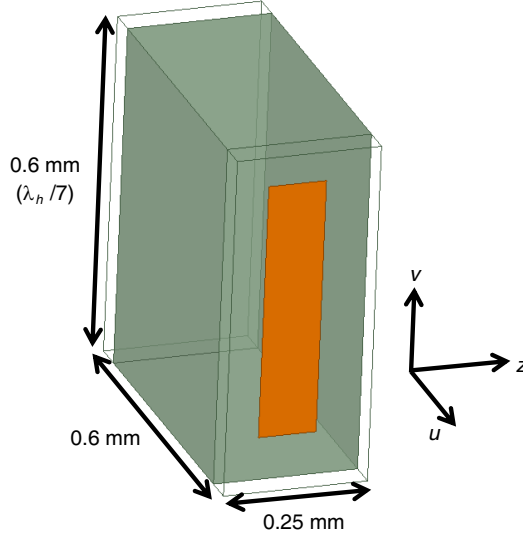
Figure 3. Unit cell of the artificial anisotropic dielectric.

unit cell thick slab with normally incident plane waves propagating in the z and u directions [22],

$$\begin{pmatrix} \varepsilon_{uu} & \varepsilon_{uv} & \varepsilon_{uz} \\ \varepsilon_{vu} & \varepsilon_{vv} & \varepsilon_{vz} \\ \varepsilon_{zu} & \varepsilon_{zv} & \varepsilon_{zz} \end{pmatrix} = \begin{pmatrix} 2.45 & 0 & 0 \\ 0 & 4.1 & 0 \\ 0 & 0 & 3.2 \end{pmatrix}. \tag{10}$$

The orientation of the different layers are $\beta_1 = 9°$, $\beta_2 = 34°$, $\beta_3 = 29°$, and $\beta_4 = 87°$, for the first through fourth layers, respectively. Their thicknesses are $t_1 = 7.75\,\text{mm}$, $t_2 = 3.25\,\text{mm}$, $t_3 = 4.25\,\text{mm}$, and $t_4 = 4.0\,\text{mm}$.

Increasing the anisotropy of the waveplate is beneficial because it reduces the required thickness. In addition, it increases robustness to fabrication tolerances since the performance of a waveplate is proportional to the difference in the indices of refraction along the principal directions (i.e., $\sqrt{\varepsilon_{vv}} - \sqrt{\varepsilon_{uu}}$). To illustrate this point, consider a single waveplate illuminated at normal incidence with $\varepsilon_{uu} = 3.2$ and $\varepsilon_{vv} = 3.5$ that converts an incident linear polarization to circular polarization. If the permittivity of $\varepsilon_{vv} = 3.5$ is reduced by 5% due to fabrication tolerances, the axial ratio of the transmitted field will increase from 0 dB to 7.5 dB. However, if the designed permittivity contrast is increased such that $\varepsilon_{uu} = 2$ and $\varepsilon_{vv} = 3.5$, a 5% decrease in ε_{vv} only increases the axial ratio to 1 dB. On the other hand, the permittivity contrast should not be increased too much since this makes it more difficult to impedance match the waveplates to free space using isotropic dielectrics.

It should be noted that the cascaded waveplates cannot be simulated as a single unit cell in a periodic lattice since the principal axes of the anisotropic layers are all different. Therefore, the simulated S-parameters of the polarizer are calculated by simply cascading the S-parameters of the individual waveplates. This technique assumes the field at the boundary between two different waveplates is accurately represented by the fundamental Floquet modes, which are propagating plane waves with TE and TM polarizations. In other words, the simulation neglects evanescent coupling between the different waveplates, which is expected to contribute only minor influences to the polarizer's response Note that the circuit solver in HFSS provides a convenient method of cascading the S-parameters of the individual waveplates.

The simulated transmission coefficient and axial ratio when illuminated with an x-polarized plane wave are shown in Figure 4 for different angles of incidence. At normal incidence, the transmission coefficient (T_{Rx}) is above -1 dB between 11 GHz and 72 GHz, and the axial ratio (AR) is below 3 dB from 15 GHz to 70 GHz (4.7 : 1 bandwidth). The polarizer also performs well at oblique incidence as shown in Figures 4(b) and (c). When illuminated at $60°$ from normal incidence in the E, H, and diagonal planes, the peak axial ratio increases to 4 dB within the operating band of 15 GHz to 70 GHz. A 4 dB axial ratio corresponds to a cross-polarization level of 12.9 dB, which is satisfactory for many
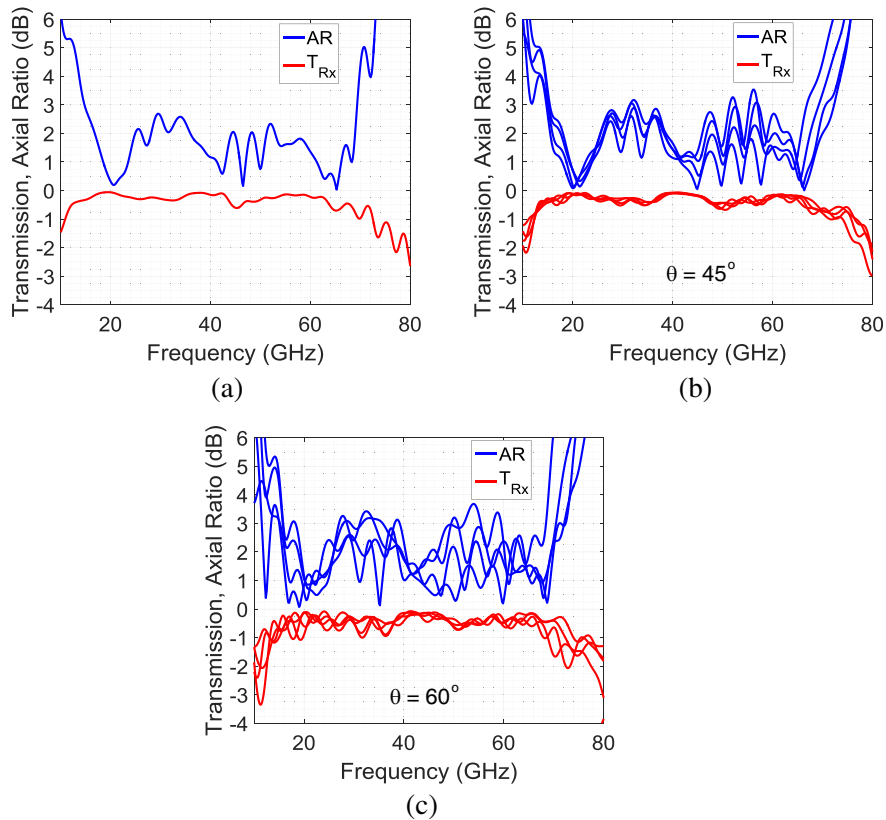
Figure 4. Simulated performance of the cascaded waveplate polarizer. (a) Simulated transmission coefficient and axial ratio from incident linear (x-polarization) to transmitted circular polarization (right-handed), when the polarizer is illuminated at normal incidence. (b), (c) Transmission coefficient and axial ratio when the polarizer is illuminated at $\theta = 45°$ and $60°$, respectively, along the E, H, and diagonal planes ($\phi = 0°$, $45°$, $90°$, $135°$).

systems. The axial ratio is below $3.7\,\mathrm{dB}$ over a $4.6:1$ and $4.4:1$ bandwidth when the angle of incidence is $45°$ and $60°$ from normal, respectively. It should be noted that while the polarizer is only designed to work for x-polarized incident waves, the symmetry of the geometry provides a similar performance when the incident wave is y-polarized. However, a y-polarized wave would be converted to left-handed circular polarization.
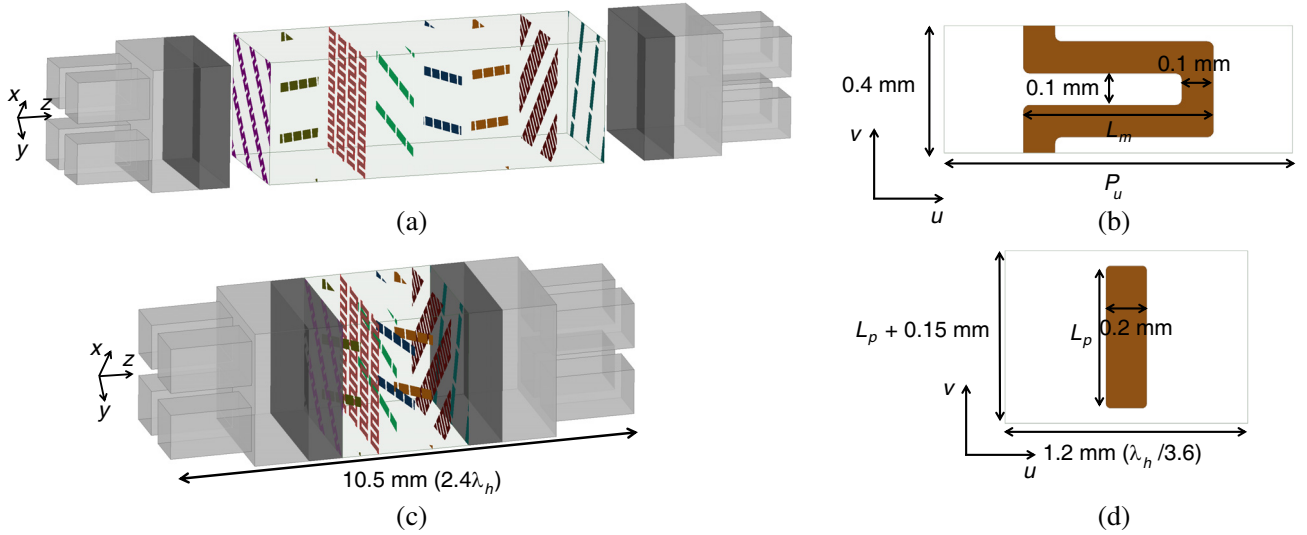
3.2. Cascaded Sheet Impedance Polarizer

The next approach to realizing an ultra-wideband polarizer is inspired by the microwave engineering community. Meanderline polarizers utilizing cascaded sheets of meandered wires were first introduced in [8]. These polarizers effectively reduce the permittivity along the direction of the wire, and increase the permittivity in the orthogonal direction, which provides an anisotropic response to control the polarization [9]. Previous polarizers typically aligned the principal axes of all layers in the $\mathbf{x} + \mathbf{y}$ and $\mathbf{x} - \mathbf{y}$ directions (i.e., $\beta = 45°$), similar to the case of linear-to-circular polarizers constructed from single waveplates. Bandwidths of up to $2:1$ have been realized with meanderline polarizers by engineering the frequency dispersion along their two principal axes [18]. However, as the bandwidth is increased, the performance at wide scan angles tends to suffer [10].

In this section, an ultra-wideband linear-to-circular polarizer is realized by modifying the conventional geometry of a meanderline polarizer. It was shown in the previous section that rotating the principal axes of the various layers increases the useful design degrees of freedom, which can be leveraged to enhance bandwidth. Therefore, the orientation of each sheet is a free variable that is

optimized. Furthermore, each sheet is not restricted to only meanderline geometries, which provides additional degrees of freedom. In other words, the layers are best represented as general, anisotropic sheet impedances.

A section of the cascaded sheet impedance polarizer is shown in Figure 5. Again, a genetic algorithm optimization in MATLAB is used to design the polarizer. The polarizer consists of impedance matching layers on the outside, and cascaded anisotropic metallic patterns printed on Rogers 4003 substrates in the middle. The permittivity of the 4003 substrate ($\varepsilon = 3.55$) is large enough to improve the performance at wide scan angles [18], but not too large such that it is not difficult to provide a broadband impedance match to free space. In total 8 patterned copper sheets are used, which are spaced 0.4 mm apart in the z-direction. This results in roughly 25 unknowns that need to be optimized: thickness and permittivity of the 3 matching layers (6 unknowns), and dimensions (roughly 11 unknowns) and orientation (8 unknowns) of the patterned metallic sheets. Again, the cost function given by (9) is used, which minimizes insertion loss and axial ratio over the operational bandwidth at normal and oblique angles of incidence.

Figure 5. Cascaded sheet impedance polarizer. (a) Section of the cascaded sheet impedance polarizer with the impedance matching layers separated from the cascaded metallic sheets, and the sheets expanded in the z-direction by a factor of 3 for clarity. (b) Meanderline geometry that exists on the first, third, and seventh sheets. (c) To-scale picture of the polarizer. (d) Patch geometry used on second, fourth, fifth, sixth, and eighth layers.

Two different metallic geometries are considered for each sheet: meanderline and metallic patches, as shown in Figures 5(b) and (d). Parametric sweeps were performed using ANSYS HFSS to extract the anisotropic sheet impedances of the patterned metallic geometries as a function of their dimensions (L_m, P_u, and L_p) and frequency, at normal incidence. Simulations demonstrated that the sheet impedance is not a strong function of the angle of incidence. Interpolation is used to approximate the sheet impedance of geometries that are not explicitly simulated. The dimension L_m primarily controls the inductance of the meanderline in the v-direction, while P_u determines the capacitance in the u-direction. The dimension L_p primarily affects the capacitance of the patch along the v-direction Again, the u and v directions correspond to the principal axes of each sheet, which are rotated by an angle β relative to the global xy coordinate system. The simulated sheet impedances are inserted into a MATLAB routine that analytically calculates the S-parameters of the cascaded structure [23, 24]. This routine is used by the genetic algorithm to optimize the dimensions and orientation of each sheet.

A brute force sweep is used to determine which sheets utilize meanderline geometries and which sheets utilize patches. First, every sheet is forced to be of the metallic patch geometry, and the genetic algorithm finds the minimum cost for this case by optimizing L_p, and β of each sheet, as well as the

permittivity and thickness of the impedance matching layers. Then the first sheet is replaced with the meanderline geometry and again the minimum cost is calculated using the genetic algorithm. This process is repeated until every possible combination of meanderline and patch geometry is considered, of which there are a total of $2^8 = 256$ combinations. At the end, the meanderline/patch combination

Table 1. Dimensions and orientation of the 8 different sheets comprising the cascaded sheet impedance polarizer.

Sheet#	L_{m} (mm)	P_{u} (mm)	L_{p} (mm)	β (deg.)
1	0.28	0.98	NA	5
2	NA	NA	0.63	118
3	0.60	0.84	NA	46
4	NA	NA	0.70	143
5	NA	NA	0.55	126
6	NA	NA	0.78	119
7	0.60	1.10	NA	89
8	NA	NA	0.76	6
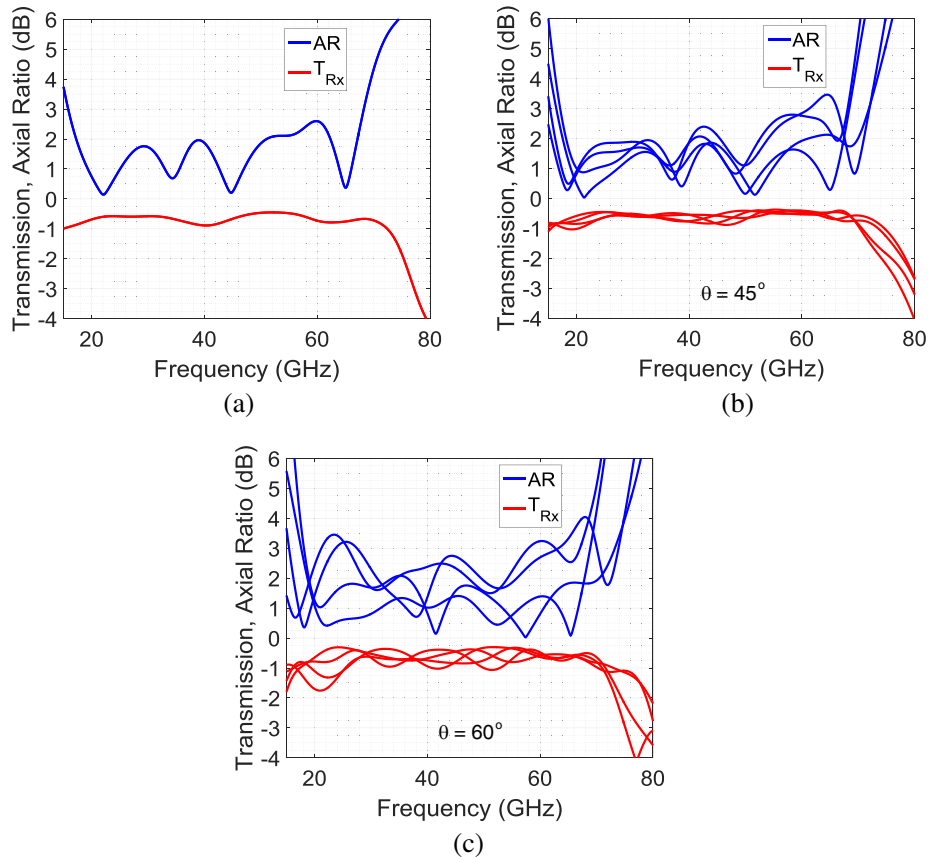
Figure 6. Simulated performance of the cascaded sheet impedance polarizer. (a) Simulated transmission coefficient and axial ratio from incident linear (x-polarization) to transmitted circular polarization (right-handed), when the polarizer is illuminated at normal incidence. (b), (c) Transmission coefficient and axial ratio when the polarizer is illuminated at $\theta = 45°$ and $60°$, respectively, along the E, H, and diagonal planes ($\phi = 0°$, $45°$, $90°$, $135°$).

with the lowest calculated cost is chosen. The optimal combination utilizes meanderline geometries on the first, third, and seventh sheets. However, it should be noted that many other options provided a similar performance. The entire optimization process required on the order of few days to complete with a 24 core CPU running at 2.5 GHz.

The optimized dimensions of each patterned metallic sheet are shown in Table 1. The effective permittivities of the impedance matching layers shown in Figure 5(a) are 1.3, 1.8, and 3.0, with thicknesses equal to 1.8 mm, 1.2 mm, and 0.75 mm, respectively.

Again it was not possible to rigorously simulate the entire polarizer using a full-wave solver. Instead, the S-parameters of the different layers are cascaded together using the circuit solver in HFSS to calculate the S-parameters of the overall structure. Full wave simulations of similar geometries that are periodic verified that simply cascading S-parameters provides an accurate estimate of the overall performance. In other words, evanescent coupling between the different layers can be neglected for these cells sizes and interlayer spacing. The simulated performance is shown in Figure 6. At normal incidence, the transmission coefficient (T_{Rx}) is above -1 dB between 15 GHz and 72 GHz, and the axial ratio is below 3 dB from 16 GHz to 68 GHz (4.2 : 1 bandwidth). Again, the polarizer performs well at oblique incidence. When illuminated at 60° from normal incidence in the E, H, and diagonal planes, the peak axial ratio increases to 4 dB within the operating band. The axial ratio is below 3.5 dB over a 4.1 : 1 and 3.7 : 1 bandwidth when the angle of incidence is 45° and 60° from normal, respectively. It should be noted that this polarizer does not efficiently convert incident y-polarized waves into circular polarization, in contrast to the majority of previously published polarizers. This is because the first sheet has a low inductance in the y-direction, which acts as a wire-grid polarizer that reflects y-polarized waves.

4. MEASUREMENTS

4.1. Experimental Setup

Both linear-to-circular polarizers were fabricated and measured using the Gaussian beam telescope shown in Figure 7 [25]. This system generates an incident Gaussian beam with beam waist diameter roughly equal to 3λ, which significantly reduces the required fabricated area compared to the case where a single lens or no lenses are used. The system operates between 15 GHz and 110 GHz. The Gaussian beam telescope consists of 2 linearly polarized standard gain horn antennas on either side of the polarizer under test. The horns have a high gain (~ 23 dB), and their radiated beams are quasi-Gaussian (85% coupling to the fundamental Gaussian mode). In order to characterize the polarizers across the wide operating bandwidth, four different standard gain horn antennas were used to cover the K, Ka, V, and W bands. The horns are connected to a 2-port network analyzer that is integrated with frequency extenders to allow for measurements of the S-parameters up to 110 GHz. The system utilizes 4 plano-
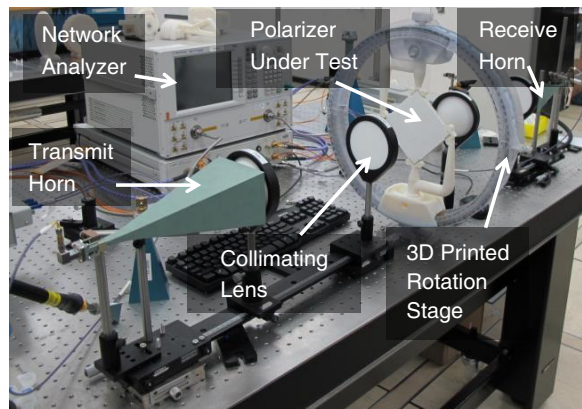

Figure 7. Gaussian beam telescope used to characterize the fabricated polarizers.

convex Teflon lenses with 100 mm diameters and 150 mm focal lengths. The lenses are separated from each other by the sum of their focal lengths (300 mm), which generates a collimated quasi-Gaussian beam at the center of the system with unity magnification at all operating frequencies [25]. The polarizers are mounted on a 3D printed rotation stage that allows for measuring the transmission coefficients at normal incidence and oblique incidence, along different planes (e.g., E, H, and diagonal planes). The beam waist diameter at the lower operating frequencies (15 GHz) is calculated to be ~ 50 mm, and it reduces as the frequency increases. Therefore, the cross sectional diameter of the polarizer needs to be at least 50 mm. Note that orienting the polarizer for measurements at oblique angles reduces the effective cross sectional area seen by the incident Gaussian beam. For example, a 60° scan angle effectively reduces the fabricated polarizer's area by half.

Linearly polarized horn antennas are used to measure the polarizers. However, characterizing the linear-to-circular transmission matrix requires knowledge of the transmitted field along two independent polarizations. Conceptually, the simplest method of characterizing the transmitted field is to first orient the receive horn to receive x-polarization and then rotate the horn by 90° to receive y-polarization. Once T_{xx} and T_{yx} are known, it is straightforward to calculate T_{Rx}, T_{Lx}, or equivalently the transmitted axial ratio. However, this approach can be inaccurate since the phase center of the receive horn can easily shift when it is physically rotated. Therefore an alternative approach is taken here. First, the two horns are oriented to measure T_{xx}. To measure an additional component of the transmitted polarization, a wire-grid polarizer oriented along the $\mathbf{x} + \mathbf{y}$ direction is inserted into the path of the Gaussian beam, after the polarizer under test. The transmission coefficients of the wire-grid polarizer along its two principal axes are independently measured so that its presence can be properly calibrated. By utilizing measurements with and without the wire-grid polarizer in the beam's path, it is possible to extract the transmitted field along two independent polarizations. These measurements are used to characterize the two most relevant characteristics of the fabricated polarizers: T_{Rx} and transmitted axial ratio.

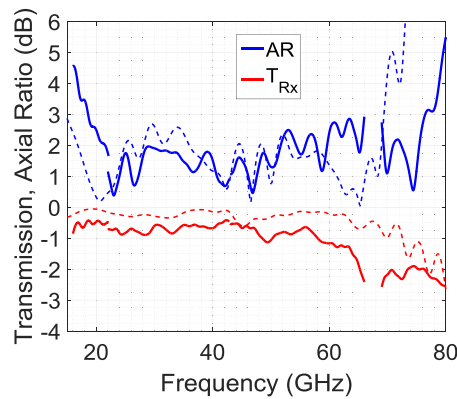### 4.2. Cascaded-Waveplate Polarizer

The cascaded waveplate polarizer is fabricated by stacking together chemically etched printed-circuit-boards, as shown in Figure 8. One of the fabricated PCBs for the first waveplate is shown in Figure 8(a). This PCB is stacked together with 83 identical PCB's in the u-direction (see Figure 3) to realize the first waveplate. The designed 0.1 mm air gap between the stacked PCBs (in the u-direction) is realized by placing 0.1 mm shims between the boards at their edges. The same process is used to realize the other three waveplates as well. The 4 different cascaded waveplates are shown in Figure 8(b). They are spread apart in the figure for clarity. 3D printed holders support each PCB in the proper orientation. Due to
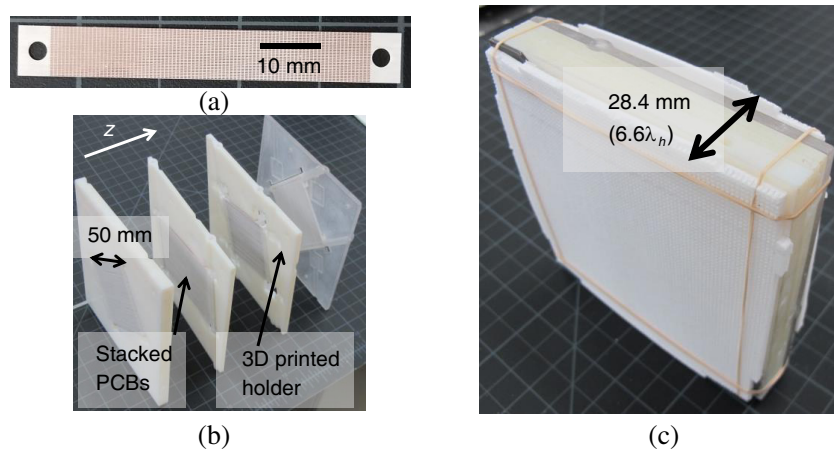
Figure 8. Fabricated cascaded waveplate polarizer. (a) One of 83 PCBs used to realize the first waveplate. (b) The 4 anisotropic waveplates expanded from each other for clarity. Each waveplate is supported by a 3D printed holder. (c) Fully assembled cascaded waveplate polarizer.

limited time and resources, the fabricated diameter of the cascaded waveplate polarizer is only 50 mm. This diameter is roughly equal to the incident Gaussian beam size at the lower operating frequencies Therefore, the polarizer is not large enough to be characterized at oblique angles of incidence. The overall size of the polarizer including the 3D printed PCB holders is 120 mm × 120 mm × 28.4 mm.

The cascaded waveplate polarizer's measured and simulated transmission coefficients (T_{Rx}) and axial ratios (AR) at normal incidence are shown in Figure 9. There is good agreement between measurement and simulation. The gap in measured frequencies at 67 GHz corresponds to the location where the network analyzer switches modes between using internal signal generators (below 67 GHz) and external frequency extenders (above 67 GHz). The measured axial ratio is below 3 dB between 19 GHz and 76 GHz (4 : 1 bandwidth), and the insertion loss is below 2.5 dB over this frequency range. The insertion loss of the measurements is about 0.5 dB larger than simulations, which could be due to fabrication tolerances, metal surface roughness, and/or air gaps between the 4 different waveplate sections and impedance matching layers.
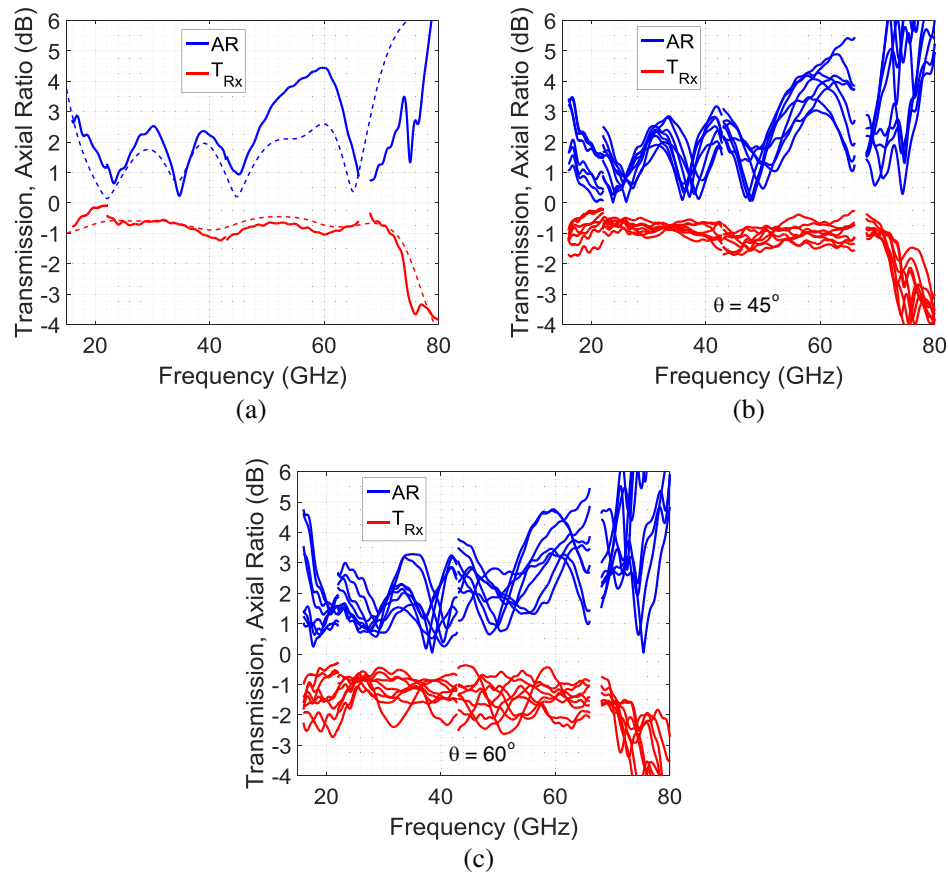

Figure 9. Measured transmission coefficient and axial ratio of the cascaded waveplate polarizer when the polarizer is illuminated at normal incidence. Dashed lines indicate simulated response. The polarizer was too small to characterize at oblique angles of incidence using the Gaussian beam telescope shown in Figure 7.

4.3. Cascaded Sheet Impedance Polarizer

The cascaded sheet impedance polarizer is fabricated using standard PCB processing techniques. Each sheet is chemically etched and then bonded together. The fabricated sheets before bonding are shown in Figure 10(a). The finished polarizer after bonding and securing the impedance matching layers is shown in Figure 10(b). The dimensions of the cascaded sheet impedance polarizer are 120 mm × 120 mm × 10.5 mm.

(a)   (b)
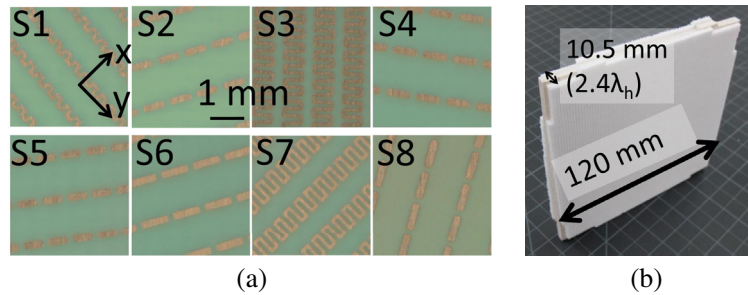
Figure 10. Fabricated cascaded sheet impedance polarizer. (a) Metallic patterns of the 8 cascaded sheets before bonding. (b) Fully assembled polarizer.
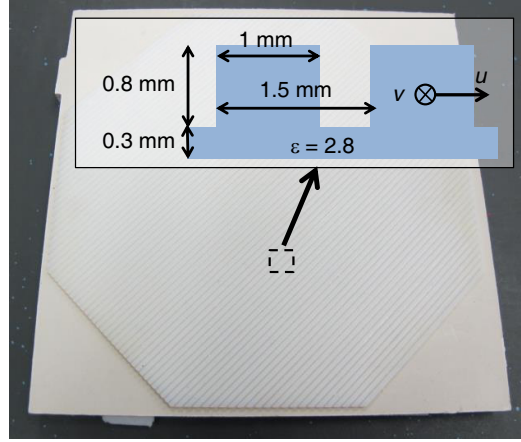
Figure 11. Measured performance of the cascaded sheet impedance polarizer. (a) Transmission coefficient and axial ratio when the polarizer is illuminated at normal incidence. Dashed lines indicate simulated response. (b), (c) Transmission coefficient and axial ratio when the polarizer is illuminated at $\theta = 45°$ and $60°$, respectively, along the E, H, and diagonal planes ($\phi = 0°$, $45°$, $90°$, $135°$, $180°$, $225°$, $270°$, $315°$ planes).

The measured and simulated performances of the cascaded sheet impedance polarizer are shown in Figure 11(a) for normal incidence. The measured insertion loss is below 1.5 dB between 16 GHz and 73 GHz, and the axial ratio is below 4.5 dB over this frequency range. There is reasonable agreement between simulation and measurement. The larger measured axial ratio at 60 GHz is attributed to fabrication tolerances. The cascaded sheet impedance polarizer was also characterized at oblique angles of incidence ($\theta = 45°$, $60°$), along the E, H, and diagonal planes ($\phi = 0°$, $45°$, $90°$, $135°$, $180°$, $225°$, $270°$, $315°$ planes). The performance only slightly degrades as the angle of incidence is increased to $45°$ from normal, as shown in Figure 11(b). At $60°$ from normal, the average insertion loss and axial ratio increases by roughly 1 dB compared to the broadside case. Therefore, the performance of the polarizer is quite robust to illumination at different angles of incidence.

4.4. Refined Cascaded Sheet Impedance Polarizer

For many applications, an axial ratio below 3 dB is desired. Unfortunately, fabrication tolerances increased the axial ratio of the cascaded sheet impedance prototype to 4.5 dB near 60 GHz. The performance could likely be improved by exploiting statistical variations in the fabrication process. Many polarizers could be fabricating and measured, and the polarizers with best performance could be picked out. However, this process would be expensive and time consuming for demonstrating a proof-of-concept.

Figure 12. Fabricated grating to refine the performance of the cascaded sheet impedance polarizer. Inset shows a side-view of the designed dielectric grating, which imparts a 7° transmitted phase difference between u and v polarizations.
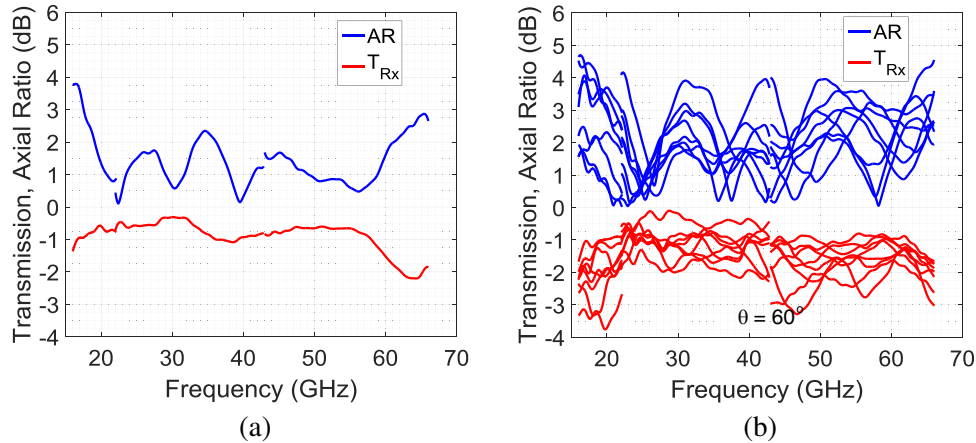
Figure 13. Measured performance of the cascaded sheet impedance polarizer when the dielectric grating is added to refine the performance. (a), (b) Transmission coefficient and axial ratio at normal incidence and 60° scan angles, respectively.

Instead, the fabricated polarizer is refined by adding an additional anisotropic layer to compensate for the higher axial ratio near 60 GHz. The 3D printed dielectric grating made from Vero White ($\varepsilon = 2.8$), shown in Figure 12, is embedded within the impedance matching layers (sandwiched between the $\varepsilon = 3$ and $\varepsilon = 1.8$ layers). A side view of the designed grating is shown in the inset. The grating generates a simulated relative phase shift difference of 7° between the u and v polarizations at 60 GHz, which in turn brings the transmitted phase shift difference between x and y polarizations closer to the ideal 90° at the higher operating frequencies. The phase shift difference between u and v polarizations is directly proportional to the frequency. Therefore, the additional grating negligibly affects the performance at the lower operating frequencies. The measured performance at normal incidence and 60° scan angles is shown in Figure 13. The presence of the dielectric grating keeps the axial ratio below 3 dB from 17 GHz to 66 GHz at normal incidence. Again, the polarizer's performance only marginally degrades when illuminated at wide scan angles as shown in Figure 13(b). However, it should be noted that the dielectric grating does increase the insertion loss at some frequencies and angles of incidence. This process of fabricating an additional 3D printed dielectric layer to refine the performance of polarization controlling devices is extremely simple and inexpensive.

5. SUMMARY

Ultra-wideband linear-to-circular polarizers that work at wide scan angles are presented at mm-wave frequencies. The polarizers are on the order of a few wavelengths in thickness to maintain a 3 dB axial ratio and 1 dB insertion loss over a 4 : 1 bandwidth. Both polarizers rely on a genetic algorithm to optimize roughly 20 design variables. The optimizations converge reasonably fast (on the order of hours) since a combination of analytic modeling and full wave simulation is used rather than purely full wave simulations

The cascaded waveplate polarizer is particularly simple to design since it is accurately modeled using effective material parameters whose response can be calculated analytically. The bandwidth of this polarizer could be increased further by simply adding more layers. However, it requires a nonstandard fabrication process and is many wavelengths in thickness, which can be undesirable for some applications. The cascaded sheet impedance polarizer is significantly thinner and easier to fabricate than the cascaded waveplate polarizer. However, the cascaded sheet impedance polarizer is more difficult to design since full wave simulations need to be integrated into the optimization process.

It is likely that the performance of both devices can be improved further by increasing the degrees of freedom. In particular additional layers could be added at the expense of increased thickness. The cascaded waveplate polarizer could also benefit from considering additional metallic geometries other than patches and meanderlines. A particularly nice feature of design by optimization is that modifying the cost function makes it straightforward to tradeoff between relevant design parameters such as maximum scan angle, bandwidth, size, and weight. For example, the goal here was to realize axial ratios around 3 dB while minimizing insertion loss for wide bandwidth and angles of incidence. However, many applications have more stringent requirements on axial ratio and insertion loss (e.g., axial ratios below 1 dB), which could be realized by modifying the cost function. Alternatively, the proposed design process could be applied a variety of other polarization transforming devices to significantly increase their bandwidth as well [23, 26].

REFERENCES

1. Pancharatnam, S., "Achromatic combinations of birefringent plates," *Proceedings of the Indian Academy of Sciences*, Vol. 41, 137–144, 1955.
2. Masson, J.-B. and G. Gallot, "Terahertz achromatic quarter-wave plate," *Optics Lett.*, Vol. 31, 265–267, 2006.
3. Pisano, G., G. Savini, P. A. R. Ade, V. Haynes, and W. K. Gear, "Achromatic half-wave plate for submillimeter instruments in cosmic microwave background astronomy: Experimental characterization," *Applied Optics*, Vol. 45, 6982–6989, 2006.
4. Pfeiffer, C. and A. Grbic, "Millimeter-wave transmitarrays for wavefront and polarization control," *IEEE Trans. on Microwave Theory and Techniques*, Vol. 61, 4407–4417, 2013.
5. Abadi, S. M. A. M. H. and N. Behdad, "Wideband linear-to-circular polarization converters based on miniaturized-element frequency selective surfaces," *IEEE Transactions on Antennas and Propagation*, Vol. 64, 525–534, 2016.
6. Lin, B., J.-L. Wu, X.-Y. Da, W. Li and J.-J. Ma, "A linear-to-circular polarization converter based on a second-order band-pass frequency selective surface," *Applied Physics A*, Vol. 123, 43, 2017.
7. Li, H.-P., G.-M. Wang, J.-G. Liang, and X.-J. Gao, "Wideband multifunctional metasurface for polarization conversion and gain enhancement," *Progress In Electromagnetics Research*, Vol. 155, 115–125, 2016.
8. Young, L., L. Robinson, and C. Hacking, "Meander-line polarizer," *IEEE Transactions on Antennas and Propagation*, Vol. 21, 376–378, 1973.
9. Lerner, D., "A wave polarization converter for circular polarization," *IEEE Transactions on Antennas and Propagation*, Vol. 13, 3–7, 1965.
10. Chu, R.-S. and K.-M. Lee, "Analytical method of a multilayered meander-line polarizer plate with normal and oblique plane-wave incidence," *IEEE Transactions on Antennas and Propagation*, Vol. 35, 652–661, 1987.

11. Zhang, W., J.-Y. Li and J. Xie, "A broadband circular polarizer based on cross-shaped composite frequency selective surfaces," *IEEE Transactions on Antennas and Propagation*, 2017, DOI 10.1109/TAP.2017.2735459.

12. Fartookzadeh, M., "Design of metamirrors for linear to circular polarization conversion with super-octave bandwidth," *Journal of Modern Optics*, Vol. 64, 1854–1861, 2017.

13. Fartookzadeh, M., "Multi-band metamirrors for linear to circular polarization conversion with wideband and wide-angle performances," *Applied Physics B*, Vol. 123, 115, 2017.

14. Yariv, A. and P. Yeh, *Optical Waves in Crystals*, Wiley, New York, 1984.

15. Balanis, C. A., *Antenna Theory: Analysis and Design*, John Wiley & Sons, Inc., Hoboken, New Jersey, 2005.

16. Ludwig, A., "The definition of cross polarization," *IEEE Transactions on Antennas and Propagation*, Vol. 21, 116–119, 1973.

17. Thor Labs, https://www.thorlabs.com/.

18. Munk, B. A., *Finite Antenna Arrays and FSS*, John Wiley & Sons, 2003.

19. Pfeiffer, C. and A. Grbic, "Emulating nonreciprocity with spatially dispersive metasurfaces excited at oblique incidence," *Phys. Rev. Lett.*, Vol. 117, 077401, 2016.

20. Brakora, K. F., J. Halloran, and K. Sarabandi, "Design of 3-D monolithic MMW antennas using ceramic stereolithography," *IEEE Transactions on Antennas and Propagation*, Vol. 55, No. 3, 790–797, 2007.

21. Akbari, M., M. Farahani, A.-R. Sebak, and T. Denidni, "Ka-band linear to circular polarization converter based on multilayer slab with broadband performance," *IEEE Transactions on Antennas and Propagation*, 2017, DOI 10.1109/ACCESS.2017.2746800.

22. Chen, X., T. M. Grzegorczyk, B.-I. Wu, J. Pacheco, Jr., and J. A. Kong, "Robust method to retrieve the constitutive effective parameters of metamaterials," *Phys. Rev. E*, Vol. 70, 016608, 2004.

23. Pfeiffer, C. and A. Grbic, "Bianisotropic metasurfaces for optimal polarization control: Analysis and synthesis," *Phys. Rev. Applied*, Vol. 2, 044011, 2014.

24. Ericsson, A. and D. Sjoberg, "Design and analysis of a multilayer meander line circular polarization selective structure," *IEEE Transactions on Antennas and Propagation*, Vol. 65, 4089–4101, 2017.

25. Goldsmith, P. F., "Quasi-optical techniques," *Proceedings of the IEEE*, Vol. 80, 1729–1747, 1992.

26. Ericsson, A., J. Lundgren, and D. Sjöberg, "Experimental characterization of circular polarization selective structures using linearly single-polarized antennas," *IEEE Transactions on Antennas and Propagation*, Vol. 65, 4239–4249, 2017.